Chapter 5

Quantitation of Glucocorticoid Receptor DNA-binding dynamics by Single-Molecule Microscopy and FRAP

Femke L. Groeneweg[1], Martin E. van Royen[2], Suzanne Fenz[3,4], Jurrien Prins[1,5], Bart Geverts[2], E. Ron de Kloet[1], Adriaan B. Houtsmuller[2], Thomas S. Schmidt[3], Marcel J.M. Schaaf[5]

An adaptation of this chapter is published as:

Quantitation of glucocorticoid receptor DNA-binding dynamics by single-molecule microscopy and FRAP. (2014) PloSOne (3):e90532

1 Department of Medical Pharmacology, Leiden University / LUMC, Leiden, The Netherlands.
2 Department of Pathology, Erasmus MC, Rotterdam, The Netherlands.
3 Physics of Life Processes, Institute of Physics, Leiden University, Leiden, The Netherlands.
4 Cell & Developmental Biology, Biocenter, Würzburg University, Würzburg, Germany.
5 Molecular Cell Biology, Institute of Biology, Leiden University, Leiden, The Netherlands.

Recent advances in live cell imaging have provided a wealth of data on the dynamics of transcription factors. However, a consistent quantitative description of these dynamics, explaining how transcription factors find their target sequences in the vast amount of DNA inside the nucleus, is still lacking. In the present study, we have combined two quantitative imaging methods, single-molecule microscopy and fluorescence recovery after photobleaching, to determine the mobility pattern of the GR, a ligand-activated transcription factor. For dexamethasone-activated GR, both techniques showed that approximately half of the population is freely diffusing, while the remaining population is bound to DNA. Of this DNA-bound population about half the GRs appeared to be bound for short periods of time ($\sim$0.7 s) and the other half for longer time periods ($\sim$2.3 s). Inactive receptors (mutant or antagonist-bound receptors) show a decreased DNA binding frequency and duration, but also a higher mobility for the diffusing population. Likely, very brief ($\sim$1 ms) interactions with DNA induced by the agonists underlie this difference in diffusion behavior. Surprisingly, different agonists also induce different mobilities of both receptors, presumably due to differences in ligand-induced conformational changes and receptor complex formation. In summary, our data provide a consistent quantitative model of the dynamics of the GR, indicating three types of interactions with DNA, which fit into a model in which frequent low-affinity DNA binding facilitates the search for high-affinity target sequences.

5.1 Introduction

In the past decade, imaging studies of fluorescently tagged proteins inside living cells have enormously increased our understanding of transcription factor dynamics (Stenoien et al., 2001; Schaaf and Cidlowski, 2003; Stavreva et al., 2004; Schaaf et al., 2005, 2006; Hager et al., 2009; van Royen et al., 2009a, 2012; Mueller et al., 2010). These studies have shown that transcription factors display a remarkably high mobility in the nucleus. Even in its most activated state a typical transcription factor appears to be able to diffuse through the entire nucleus, and to be immobilized only transiently (Gorski et al., 2006; Biddie and Hager, 2009; Hager et al., 2009). One often-studied transcription factor is the GR. This cytoplasmically localized receptor translocates to the nucleus upon binding of naturally occurring glucocorticoids (corticosterone and cortisol) or their synthetic analogs. In the nucleus the steroid-GR complexes can bind either directly or indirectly (through interactions with other transcription factors) to DNA and alter transcription rates of responsive genes (Beato and Sanchez-Pacheco, 1996; Heitzer et al., 2007; Datson et al., 2008). Like other transcription factors, ligand-activated GRs display a high mobility within the nucleus in FRAP studies (McNally et al., 2000; Schaaf and Cidlowski, 2003; Stavreva et al., 2004; Schaaf et al., 2005; Mueller et al., 2008). Using GR mutants with reduced DNA-binding capacity or antagonist-bound GR, a negative correlation was shown between GR mobility and the capacity to initiate transcription (Schaaf and Cidlowski, 2003; Elbi et al., 2004; Stavreva et al., 2004).

In the last decade many new imaging techniques have become available that open possibilities for more detailed quantifications of protein dynamics (Stasevich et al., 2010b; Li and Xie, 2011; Mazza et al., 2012; Gebhardt et al., 2013). One such approach is single-molecule microscopy (SMM). In SMM, conventional wide-field fluorescence microscopy is combined with a fast, ultra-sensitive CCD camera to enable the visualization of single fluorescent molecules with high temporal ($\sim$6 ms) and spatial (positional accuracy of $\sim$40 nm) resolution (Lord et al., 2010; Li and Xie, 2011). Initially, SMM was used to study the mobility patterns of membrane proteins (Lommerse et al., 2004; Suzuki et al., 2005; Schaaf et al., 2009; Kasai et al., 2011; Serge et al., 2011), and it has now been adapted for studies of nuclear proteins (Yang et al., 2004; Yang and Musser, 2006) and transcription factors (Elf et al., 2007; Li and Elf, 2009; Mazza et al., 2012), including a recent study on the GR (Gebhardt et al., 2013). Importantly, the analysis of single-molecule displacement patterns gives a very direct and unbiased picture of protein dynamics (Schutz et al., 1997; Semrau and Schmidt, 2007). For the more conventional population-based approaches, the correct control for confounding factors such as laser irregularities and the requirement of many *a priori* assumptions and independent variables introduce bias in the outcomes and have been a major challenge for the field (Mueller et al., 2008, 2010; van Royen et al., 2009a,b). To control for any confounding factors that might still exist in the SMM analysis, we combine SMM analysis with an established Monte Carlo quantification approach of FRAP imaging (Farla et al., 2004; van Royen et al.,

2009b). The combination with FRAP not only gives independent cross-validation of the SMM predictions, but also enables a quantification of protein kinetics over a longer time frame than SMM.

Our data show that this combination of techniques provides a very consistent quantitative analysis of GR dynamics. Based on our data, we can distinguish three states of agonist-activated GR molecules; one diffusing state and two DNA-bound states, one with short (< 1 sec) and one with a longer (2–4 sec) binding duration. Transcriptionally inactive GR variants show a reduction in the frequency and in the duration of both DNA binding events, and an increase in the diffusion rate of the diffusing population. This suggests that within this diffusing population an additional very brief DNA-binding event is hidden, resulting in a lower effective diffusion rate.

5.2 Methods

Cell culture and plasmids

In most experiments, COS-1 cells were used, grown in high-glucose D-MEM (Invitrogen) supplemented with 10 % FBS and 1 % penicillin/streptomycin (both GIBCO). 24 h prior to transfection, cells were plated on sterile coverglasses (25 mm diameter). Cells were transfected with the TransIT-COS kit (Mirus) according to the manufacturer's instructions at a concentration of 500 ng DNA / 10 cm^2. Transfected cells were used in experiments 2–5 days after transfection. For one experiment, Hep3B cells were used, stably transfected with the pEYFP-hGR expression vector (Schaaf and Cidlowski, 2003). These cells were grown in α-MEM (Cambrex), supplemented with 5 % FBS, 2 mM L-glutamine, 1 % Penicillin/Streptomycin and 600 µg/ml G418 (Invitrogen). The generation of the pEYFP-GR plasmid, the three deletion mutants of this vector (pEYFP-GR Δ9–385, pEYFP-GR Δ428–490, and pEYFP-GR Δ551–777, and the point mutant (pEYFP-GR F623A) have been described previously (Schaaf and Cidlowski, 2003; Schaaf et al., 2005).

Compounds

The following ligands were used in these studies: dexamethasone, corticosterone, cortisol, Δ-fludrocortisone (*1,4-pregnadien-9α-fluoro-11β,17,21-triol-3,20-dione*), prednisolone (*1,4-pregnadien-11β,17,21-triol-3,20-dione*) and RU486 (*4,9-estradien-17α-propynyl, 11β-[4-dimethylaminophenyl]-17β-ol-3-one*). All steroids were purchased from Sigma-Aldrich and diluted in 100 % EtOH to a concentration of 1 mM. All steroids were used at a final concentration of 1 µM in the medium.

Single molecule microscopy

For all SMM experiments, COS-1 cells were grown on coverslips and transiently transfected with the corresponding plasmid (500 ng / 10 cm^2) 3–5 days prior to analysis. Before SMM recordings, cells were exposed to 1 µM of corresponding hormones for 3–6 h. For SMM measurements, this medium was replaced by serum- and phenol red-free D-MEM medium (Invitrogen), which is also supplemented with 1 µM of the corresponding hormone. Subsequently, cells were transferred to the SMM setup and imaged for up to 90 min at 35 °C. A wide-field

fluorescence microscope (Axiovert 100TV, Zeiss) was used, equipped with a 100× / 1.4NA oil-immersion objective (Zeiss). A region-of-interest (ROI) of 50 × 50 pixels (pixel size of 220 nm) was selected. The sample was illuminated by an 514 nm argon laser at an intensity of 2 kW/cm^2. The pulse length of 3 ms was controlled by an acusto-optical tunable filter (AA optoelectronics, France). The EYFP fluorescence signal was detected through a combination of filters (DCLP530, HQ570/80 (Chroma Technology, Brattleboro, VT) and OG530-3 (Schott, Mainz, Germany)), by a liquid-nitrogen cooled CCD camera (Princeton Instruments, Trenton, NJ), camera read out and AOTF timing were tightly controlled. Healthy and moderately fluorescent nuclei were selected and then photobleached until single fluorescence intensity peaks could be distinguished. The position of each individual molecule was fitted with the intensity profile of a 2D Gaussian model of EYFP peaks (Harms et al., 2001). Our peaks were identified with a signal to noise ratio of ∼8 (peak fluorescence intensity divided by the variation of the background), which resulted in a positional accuracy of ∼40 nm in the X- and Y-direction (determined by the quotient of the full-width-at-half-maximum of the Gaussian fit and the square root of the number of photons detected (Bobroff, 1986)). On average, each picture contained ∼1.5 peaks. Image sequences were recorded in series of 8 subsequent images with a time lag of either 6.25 ms or 12.5 ms (Figure 5.1C). Data on molecular dynamics were obtained for multiple step sizes. We used all time lags from 6.25 to 37.5 ms in our analysis. From each cell 180 series of 8 images were taken and data from 20 independent cells (imaged on at least 3 different days) was combined for the analysis.

PICS analysis of single-molecule kinetics

We used the Particle Image Correlation Spectroscopy (PICS) method to determine peak displacement over time (Semrau and Schmidt, 2007). In PICS, the cross-correlation between peak positions at two different time lags (for example $t = 0$ ms and $t = 6.25$ ms) is calculated. This yields the cumulative probability distribution (C_{cum}) of all 'diffusion steps' detected within 6.25 ms. C_{cum} includes both contributions from diffusing molecules as well as random correlations between unrelated molecules in the two frames. The latter follows a linear relation in the cumulative plot and was subtracted prior to further analysis. From the remaining cumulative probability function (P_{cum}) of diffusion steps l, we use population modeling to calculate diffusion characteristics of the nuclear population of YFP-GR (Figure 5.1D). Given that the population of molecules is homogeneous, a single population of displacing molecules is determined with

$$P_{\text{cum}}(l, \Delta t) = 1 - \exp\left(-\frac{l^2}{\text{MSD}_0(\Delta t)}\right) \tag{5.1}$$

Here MSD_0 is the mean square displacement of one population of molecules over the time lag. However, this one fraction model could not explain the experimental data (Figure 5.1D). Therefore a second fraction was introduced and the equation reads as follows:

$$P_{\text{cum}}(l, \Delta t) = 1 - \left[\alpha \cdot \exp\left(-\frac{l^2}{\text{MSD}_1(\Delta t)}\right)(1-\alpha) \cdot \exp\left(-\frac{l^2}{\text{MSD}_2(\Delta t)}\right)\right] \tag{5.2}$$

Where MSD_1 and MSD_2 denote the mean square displacement of the first (fast) and the second (slow) fractions respectively, and α is the fraction size of the first (fast) fraction. A two-population model fitted the experimental data with high accuracy (Figure 5.1D). Although diffusion happens in 3D, we measure only the 2D projection, and to prevent distortion of the

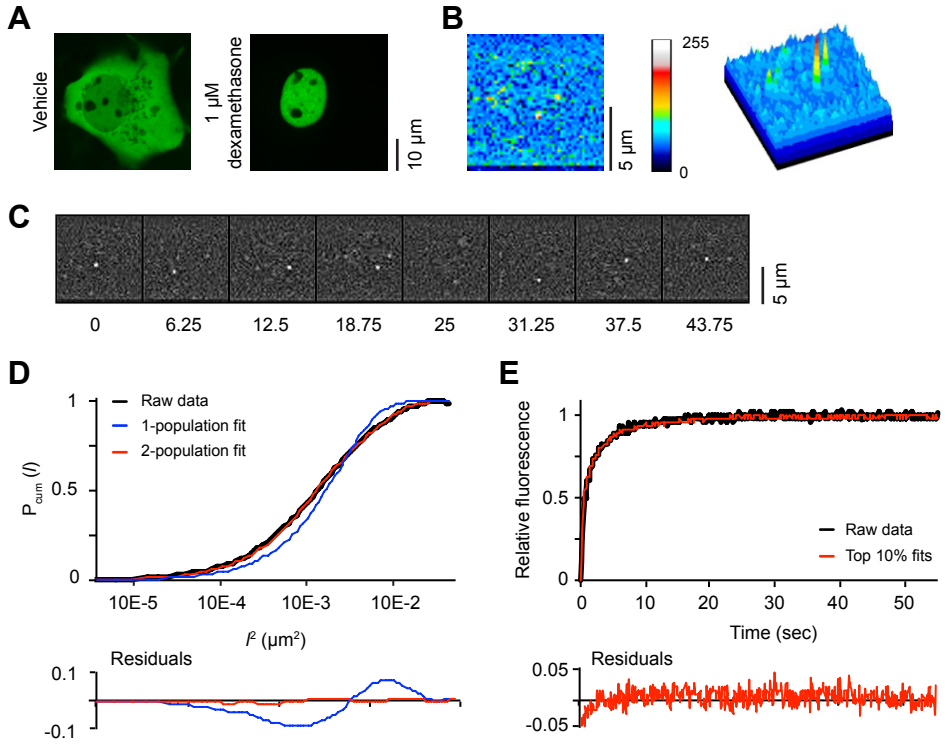

Figure 5.1: SMM and FRAP procedures
(A) Representative confocal images show complete nuclear translocation of YFP-GR after 3 hours of 1 µM dexamethasone treatment. (B) A representative CCD image of single molecules of YFP-GR after background subtraction shows two discernible Gaussian peaks of YFP fluorescence. (C) Regime for single molecule kinetics; images are taken with a time lag of 6.25 ms or 12.5 ms in 300 series of 8 per cell. In background-subtracted images, single molecules of YFP fluorescence are easily discernible. (D). PICS analysis of single molecule displacements, shown for dexamethasone-bound YFP-GR at time delay of 6.25 ms. The cumulative probability distribution as a function of the squared distance l (black line) is best fitted with a 2-population model (red line), while a 1-population model gives a suboptimal fit (blue line) ($n = 20$ cells). (E) FRAP procedure of dexamethasone-bound YFP-GR. At $t = 0$ a 100 ms bleach pulse is applied to a strip spanning the nucleus. Subsequently, FRAP recovery curves of 30 cells are recorded, combined and adjusted to baseline fluorescence (black line). Subsequently, Monte Carlo simulations are generated using a 3-population model and fitted to the combined FRAP curve. The top 10 fits are combined (red line) and show a good fit of the experimental data with small residuals.

data due to molecules 'escaping' in 3D space, we restrict ourselves to only small time lags (up to 42.5 ms). In simulation experiments, we have demonstrated that within this time from the effects of 'escaping' molecules can be neglected (data not shown). The analysis was repeated for each time lag and α, MSD_1 and MSD_2 were plotted against time (Δt). The displacements over time were best described using a free diffusion model in 2D, from which the diffusion coefficients (D_{fast} and D_{slow}) were calculated using the following equation:

$$\mathrm{MSD}_i(\Delta t) = 4 \cdot D_i \cdot \Delta t \tag{5.3}$$

OriginPro software was used to obtain weighted, linear fits, to calculate D_{fast} and D_{slow}. The fraction size α decreased slightly (on average -0.18 ± 0.03 %/ms) over increasing time lags in

all groups. Due to this effect, we always report the fraction distribution of the smallest time step (6.25 ms) as a representative of the overall fraction distribution. All analyses were first performed on all data from each treatment group pooled together ($n = 20$). Subsequently, all analyses were run again in 3 fractions ($n = 6/7$) and these 3 separate analyses are used to generate standard errors of the mean.

FRAP

For FRAP recordings, COS-1 cells were grown on coverslips and transiently transfected with 500 ng / 10 cm^2 of the corresponding plasmid and used 2–3 days after transfection. Before FRAP recordings, cells were exposed to 1 µM of the appropriate ligand for 3–6 hours in normal growth medium. For each experiment, a coverglass with transfected COS-1 cells was placed in a preheated ring and medium was replaced for empty D-MEM without phenol red, supplemented with 1 µM of the corresponding ligand. Cells were used for no longer than 90 minutes and kept at 37 °C and 5 % CO_2. We used a Zeiss LSM510 META confocal laser scanning microscope equipped with a 40× / 1.3NA oil-immersion objective, an argon laser (30 mW) and an AOTF. For FRAP analysis a narrow strip spanning the entire width of the nucleus was scanned at 514 nm excitation with short intervals (100 ms) at low laser power (0.2 %). Fluorescence intensity was recorded using a 560 nm longpass filter. After 40 scans, a high intensity (100 % laser power), 100 ms-bleach pulse at 514 nm was applied over the whole strip. Subsequently, the recovery of the fluorescence intensity in the strip was followed for another 55 seconds at 100 ms intervals. For each treatment group 30 cells were measured by FRAP on two separate days. All curves were normalized to baseline fluorescence intensity and combined.

Monte Carlo quantification of FRAP curves

The FRAP data was quantitatively analyzed by comparing the experimental data to curves generated using Monte Carlo modeling (van Royen et al., 2009b). The Monte Carlo computer simulations used to generate FRAP curves for the fit were based on a model that simulates diffusion of molecules in three dimensions and binding to immobile elements in an ellipsoidal volume. In short, simulated FRAP curves were generated with a 3-population model, containing a diffusing fraction and two bound (immobile) fractions. We take the D_{fast} obtained from SMM analysis as a fixed parameter in these simulation, leaving 4 parameters as variables: short bound fraction, long bound fraction (both ranging from 0–90 %), and time spent in short and long bound state (ranging from 0.1 s to 1 s and from 1 s to 300 s respectively). The laser bleach pulse was simulated based on experimentally derived three-dimensional laser intensity profiles, which were used to determine the probability for each molecule to get bleached considering their 3D position. The simulation of the FRAP curve was run using discrete time steps corresponding to the experimental scan interval of 21 ms. Diffusion was simulated at each new time step $t + \Delta t$ by deriving the new positions $(x_{t+\Delta t}, y_{t+\Delta t}, z_{t+\Delta t})$ of all mobile molecules from their current positions (x_t, y_t, z_t) by $x_{t+\Delta t} = x_t + G(r_1)$, $y_{t+\Delta t} = y_t + G(r_2)$, and $z_{t+\Delta t} = z_t + G(r_3)$, where r_i is a random number ($0 \leq r_i \leq 1$) chosen from a uniform distribution, and $G(r_i)$ is the inverse of a cumulative Gaussian function with $\mu = 0$ and $\sigma^2 = 2D\Delta t$, where D is the diffusion coefficient (obtained from SMM analysis). Immobilization was derived from simple binding kinetics described by:

$$\frac{k_{\text{on}}}{k_{\text{off}}} = \frac{F_{\text{imm}}}{F_{\text{mob}}} \tag{5.4}$$

where F_{imm} is the relative number of immobile molecules and $F_{\text{mob}} = 1 - F_{\text{imm}}$. The probability for each particle to become immobilized (representing chromatin-binding) is defined as:

$$P_{\text{immobilized}} = k_{\text{on}} = \frac{F_{\text{imm}}}{T_{\text{imm}} \cdot F_{\text{mob}}} \tag{5.5}$$

where T_{imm} is the characteristic time spent in the immobile state. The probability to be released is given by:

$$P_{\text{mobilized}} = k_{\text{off}} = \frac{1}{T_{\text{imm}}} \tag{5.6}$$

As our model includes two bound fractions with different immobilization times, two immobilization/mobilization probabilities were evaluated for each unit time step. In all simulations, the size of the ellipsoid was based on the average size of measured nuclei, and the FRAP region used in the measurements determined the size of the simulated bleach region. The laser intensity profile using the simulation of the bleaching step was previously derived from confocal image stacks of chemically fixed nuclei containing GFP that were exposed to a stationary laser beam at various intensities and varying exposure times. The unit time step (Δt) corresponded to the experimental sample rate of 21 ms. The number of molecules in the simulations was 10^6, which was empirically determined by producing curves that closely approximate the data with comparable fluctuations. The parameters of the top 10 best fitting Monte Carlo curves (by ordinary least squares) were averaged to represent the properties of the fractions in the experimental data.

5.3 Results

We first investigated the nuclear dynamics of the GR by SMM. We used COS-1 cells, transiently transfected with EYFP-tagged human GR (YFP-GR). This YFP-GR fusion protein was previously shown to retain a good transcriptional activity (Schaaf and Cidlowski, 2003). Before analysis, cells were exposed for 3 to 6 hours to a saturating dose (1 µM) of the high affinity GR agonist dexamethasone, which induces nuclear translocation of YFP-GR (Figure 5.1A). Nuclei were photobleached until single diffraction-limited fluorescence intensity peaks could be distinguished (Figure 5.1B). These peaks are attributed to single YFP-GR molecules as they had comparable width and intensity as fluorescence intensity peaks derived from single EYFP molecules previously observed using the same setup (Harms et al., 2001). In our current approach, EYFP molecules were identified with a positional accuracy of $\sim$40 nm in one dimension (x or y). Next, GR mobility was analyzed by assessing molecule displacements over image sequences with short time lags (6.25 ms and 12.5 ms; Figure 5.1C), using the PICS analysis method (Semrau and Schmidt, 2007). We use PICS analysis instead of single particle tracking, as PICS is less affected by blinking of YFP or overlapping trajectories of multiple molecules (Schutz et al., 1997; Semrau and Schmidt, 2007). PICS analysis calculates the cumulative probability distribution for each displacement, which is subsequently fitted with multiple-population models (Figure 5.1D, see material and methods). We use a

model with only fractions of moving molecules instead of a model encompassing a bound (immobile) fraction, because this is the more general model without *a priori* assumptions. DNA-bound and thus immobile molecules should show negligible displacement steps in this model. For YFP-GR, a one-population model was unable to describe the experimental data (Figure 5.1D), while a three-population model did not give consistent results over different time lags or resulted in two fractions with similar displacements. A two-population model fitted the observed displacements consistently, and with high accuracy, and was chosen for all analyses. Thus, we obtained the relative size and mean squared displacement (MSD) of two fractions of YFP-GR molecules that differed in their relative displacements over time.

We plotted the MSDs of the two identified fractions versus the time lag and calculated the diffusion coefficients (D_{fast} and D_{slow}; Figure 5.3B). The displacements of the "slow" fraction never exceeded our detection limit ($0.009\,\mu m^2$) by more than 2-fold and only increased marginally over time: D_{slow} of $0.03 \pm 0.01\,\mu m^2/s$. This is very similar to the slow restricted movement of chromatin (Blainey et al., 2006; Elf et al., 2007), indicating that this "slow" fraction describes DNA-bound molecules. In contrast, the remaining fraction showed > 40-fold higher displacements and a D_{fast} of $1.31 \pm 0.13\,\mu m^2/s$, representing YFP-GR molecules diffusing through the nucleus. The nuclear GR population is approximately evenly distributed over the two fractions; $55.1 \pm 2.0\,\%$ belongs to the diffusing fraction, which leaves $44.9 \pm 2.0\,\%$ as bound fraction (Figure 5.3A).

FRAP analysis of dexamethasone-bound YFP-GR

Subsequently, we employed a quantitative FRAP approach on similarly treated YFP-GR expressing COS-1 cells. In selected nuclei a small strip, spanning the width of the nucleus, was bleached with a $100\,ms$ pulse of maximal laser power. This effectively bleached most fluorescence within this area. The subsequent recovery of the fluorescence in this strip was recorded (with $100\,ms$ intervals) for 55 seconds (Figure 5.1E). Comparable to previous results (Schaaf and Cidlowski, 2003; Schaaf et al., 2005), a complete recovery of YFP-GR fluorescence was seen well within 30 seconds (Figure 5.1E). The obtained recovery curves were quantitatively analyzed by fitting them to FRAP curves generated using Monte Carlo simulations (van Royen et al., 2009a,b). Our data was best fitted with a model in which freely diffusing molecules (diffusion rates as obtained by SMM were used) show transient binding with two different durations ('short' and 'long'; Figure 5.1E). Quantitative FRAP analysis of dexamethasone-treated GR identified a diffusing fraction of $44 \pm 2\,\%$, a 'short' bound fraction of $33 \pm 2\,\%$ (average binding of $0.7 \pm 0.1\,s$) and a 'long' bound fraction of $23 \pm 2\,\%$ (average binding of $2.3 \pm 0.3\,s$) (Figure 5.3C,D). As both bound fractions in FRAP remain bound for much longer time periods than the time range used in SMM (less than $50\,ms$), these two fractions could be distinguished using FRAP, but not by SMM. Indeed, the size of the single bound fraction in SMM, is similar to the combined size of the two bound fractions identified in FRAP (com-

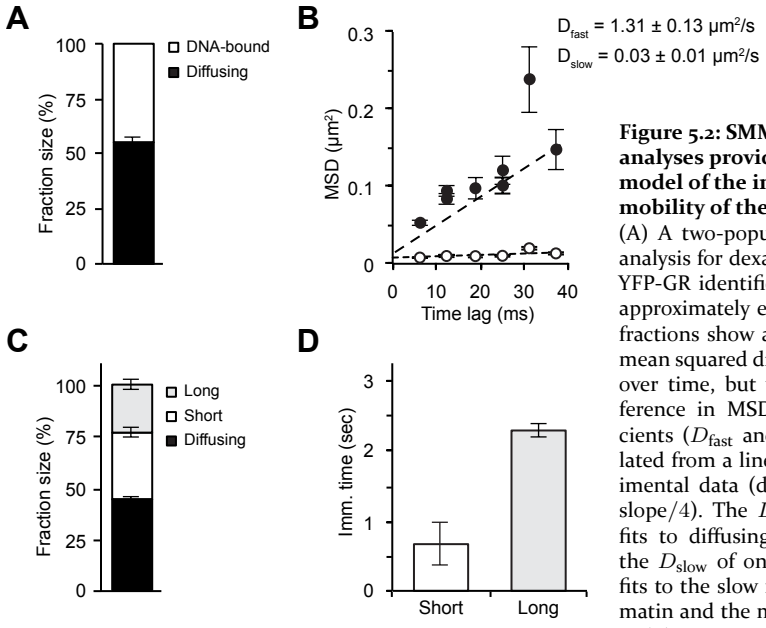

Figure 5.2: SMM and FRAP analyses provide a consistent model of the intranuclear mobility of the GR
(A) A two-population fit of SMM analysis for dexamethasone-bound YFP-GR identifies two fractions of approximately equal size. (B) Both fractions show a linear increase in mean squared displacement (MSD) over time, but with a 40-fold difference in MSD. Diffusion coefficients (D_{fast} and D_{slow}) are calculated from a linear fit of the experimental data (dashed lines; $D = \text{slope}/4$). The D_{fast} of $1.31\,\mu\text{m}^2/\text{s}$ fits to diffusing molecules, while the D_{slow} of only $0.03\,\mu\text{m}^2/\text{s}$ best fits to the slow movement of chromatin and the molecules bound to it. (C) Monte Carlo simulation of dexamethasone-bound YFP-GR with a 3-population model identifies 3 fractions of dexamethasone-bound YFP-GR; almost half of the nuclear population is diffusing, while the remainder is subdivided into two bound fractions that differ in their immobilization times. The fraction size of the diffusing fraction is similar in size as that obtained from SMM analysis. (D) Both bound fractions are only transiently immobilized, with a 3-fold difference in duration. (A and B) Data represented as best fit ± SEM (of 3 separate PICS analyses). (C and D) Data represented as average of top 10 % best fits ± SEM.

pare Figure 5.3A and 5.3C). Therefore, the mobility patterns assessed by SMM at the millisecond range are confirmed with realistic accuracy using an independent FRAP approach.

YFP-GR mobility is dependent on ligand structure

Next we used our combined SMM and FRAP approach to investigate how binding of different ligands affects GR-DNA binding dynamics. We have previously shown by FRAP that the structure of the ligand is an important determinant of GR affinity, with important roles for the 17-hydroxyl and 9-fluoro groups on the steroids, which induce a decrease in GR mobility (Schaaf and Cidlowski, 2003; Schaaf et al., 2005). In the present study, this was studied in more detail in order to investigate which of the mobility parameters were affected. Therefore, we tested a panel of GR agonists that enabled us to study the effects of the 17-hydroxyl, 9-fluoro, and 16-methyl groups and the 1,4-pregnadien structure of the A ring. We used dexamethasone (which contains all four structural elements), Δ-fludrocortisone (same structure as dexamethasone, but lacking the 16-methyl group), prednisolone (same structure as Δ-fludrocortisone, but lacking the 9-fluoro group), cortisol (same structure as prednisolone, but having a 4-pregnen instead of a 1,4-pregnadien structure),

and corticosterone (same structure as cortisol, but lacking the 17-hydroxyl group). In addition to this panel of agonists, the GR antagonist RU486 was used. Importantly, all hormones were administered at a saturating concentration (1 μM), thus the fraction of bound receptor should be similar for all ligands (Rupprecht et al., 1993; Hellal-Levy et al., 1999; Grossmann et al., 2004; Schaaf et al., 2005).

Again, the two independent experimental approaches gave a consistent pattern of fraction sizes for all 6 ligands tested. On average the size of the diffusing fractions identified with SMM and FRAP differed by only 7.8 ± 2.6 % (Table 5.1). The data show that the 16-methyl group does not affect GR mobility, but the other structural elements decrease the mobility of the receptor, indicating increased DNA binding (Figure 5.3A–C). Interestingly, this decreased mobility was reflected in all parameters measured. Both the size of the bound fractions and their respective binding time were affected, so both on- and off-rates of DNA binding were altered. In addition, the diffusion coefficient of the diffusing fraction was decreased suggesting that DNA binding results in slower diffusion of the receptor (Figure 5.3A and Table 5.1). Binding of the antagonist RU486 induces a very mobile nuclear YFP-GR (Figure 5.3A–C).

It is known that the 9-fluoro group (present on Δ-fludrocortisone and dexamethasone) creates a strong hydrogen bond with phenylalanine at position 623 of GR's ligand binding pocket (Bledsoe et al., 2002), suggesting that this amino acid is crucial in conferring the effects of the 9-fluoro-group. To test this association in our setup, phenylalanine 623 was mutated to an alanine (F623A). We tested the mobility of F623A with SMM in presence of prednisolone and Δ-fludrocortisone, which are identical except that Δ-fludrocortisone contains a 9-fluoro group and prednisolone does not. In presence of either steroid the F623A mutant translocates fully to the nuclear compartment (Figure 5.3D). Within the nucleus, no difference in F623A mobility was observed between Δ-fludrocortisone and prednisolone (Figure 5.3E). Therefore we conclude that the effect of the 9-fluoro group on mobility is indeed mediated by phenylalanine 623.

Specific receptor domains determine YFP-GR mobility

In order to elucidate the role of the different domains of GR on DNA-binding dynamics, we tested three different GR deletion mutants, each lacking one of its three functional domains. Thus, we obtained YFP-GR ΔAF-1 (lacking the N-terminal domain containing the AF-1 (amino acids 9–385)), YFP-GR ΔDBD (lacking the DNA-binding domain (amino acids 428–490)) and YFP-GR ΔLBD (lacking the ligand-binding domain (amino acids 551–777)), see Figure 5.4A. We investigated the mobility of the three deletion mutants of YFP-GR by SMM and FRAP in the presence of dexamethasone or corticosterone. All results are shown in Figure 5.4 and Table 5.1. Deletion of the AF-1 showed the smallest effect on receptor mobility. Dexamethasone binding to the ΔAF-1 mutant induces a large DNA-bound fraction and long binding times, and a slow diffusing fraction. In contrast, corticosterone binding,

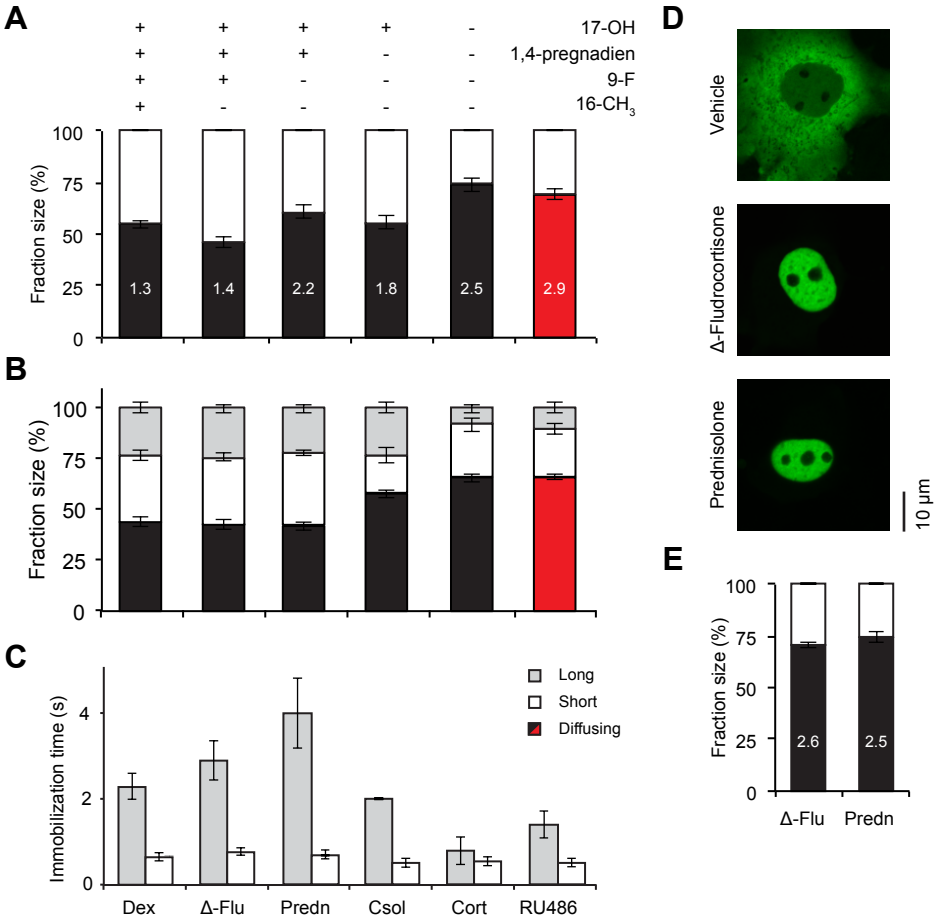

Figure 5.3: Ligand structure determines the nuclear mobility of the GR
A range of natural and synthetic agonists (black bars) and an antagonists (red bar) were tested for their effect on the intranuclear mobility of the GR by both SMM (A) and FRAP (B, C) analysis. Multiple structural elements of the steroids are associated with a reduced mobility of the receptor, with the strongest effects observed for the 9-fluoro (9-F) and the 17-hydroxyl (17-OH) groups. Altered mobility is generally reflected in all aspects of mobility: a larger bound fraction (SMM; white bars and FRAP; white and light grey bars combined), a lower diffusion coefficient (in $\mu m^2/s$, written in its corresponding bar in A) and longer immobilization times (C). (D and E) A mutation of phenylalanine 623 to alanine (F623A) prevents interactions of the 9-fluoro group of steroids within the ligand binding pocket of the GR. (D) F623A YFP-GR still translocates completely to the nucleus after 3 hours of 1 µM prednisolone or Δ-fludrocortisone treatment (E). SMM analyses of nuclear F623A YFP-GR shows that the mobility of F623A YFP-GR is highly similar after either Δ-fludrocortisone or prednisolone treatment (black bars for the diffusing fraction, with their corresponding diffusion coefficient (in $\mu m^2/s$) written within their corresponding bar). SMM: $n = 20$, FRAP: $n = 30$. Data represented as total fit ± SEM (of 3 separate PICS analyses) for SMM and as average of top 10 % fits ± SEM for FRAP. Δ-flu; Δ-fludrocortisone, dex; dexamethasone, predn; prednisolone, csol; cortisol, cort; corticosterone. The data for GR-dexamethasone is the same as in Figure 5.3.

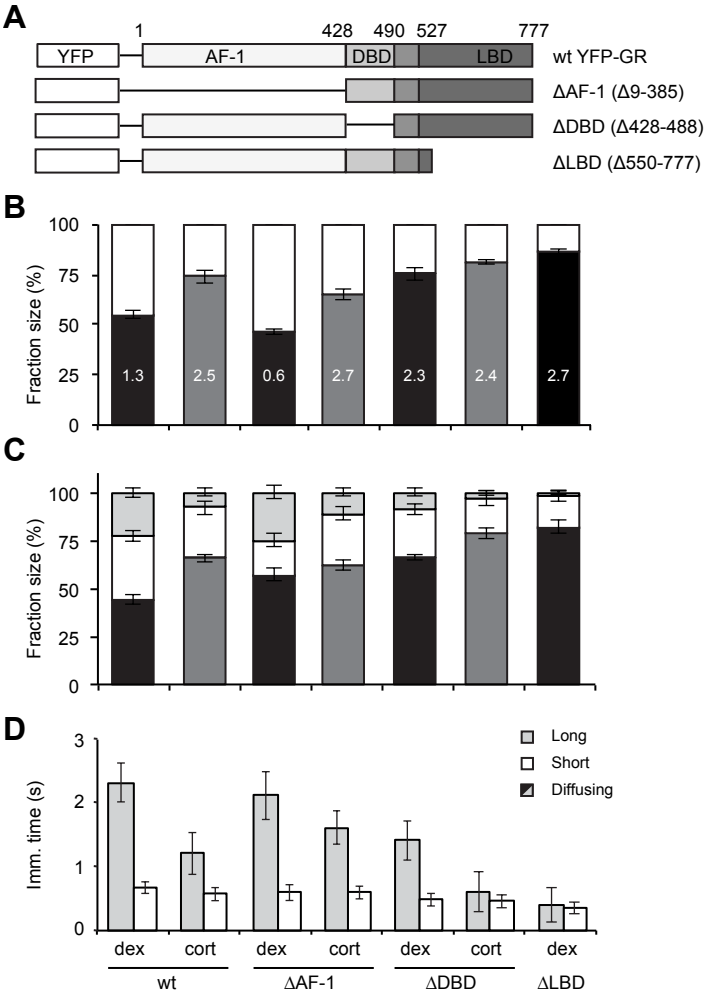

Figure 5.4: Loss of either the DNA-binding or the ligand-binding domain results in a high GR mobility
(A) Schematic representation of three functional YFP-GR deletion mutants tested. (B and C) Fraction distributions as analyzed by SMM (B) and FRAP (C). Diffusion coefficients are written within the corresponding bars in B (in $\mu m^2/s$). (D) Immobilization times of the short and long bound fractions. While loss of the AF-1 domain hardly affects GR's nuclear mobility, deletion of the DBD and especially the LBD leads to a very mobile receptor with reduced frequency and average duration of DNA-binding and a higher diffusion coefficient. SMM: $n = 20$, FRAP: $n = 30$. Data represented as total fit $\pm$ SEM (of 3 separate PICS analyses) for B and as average of top 10 % fits $\pm$ SEM for C and D. The data for wild type GR is the same as in Figure 5.3.

results in a much faster receptor with less stable DNA-binding (Figure 5.4). Thus, without its N-terminal domain, the GR's intranuclear mobility is still differently affected by high and low affinity agonists and its mobility is similar to the wild type receptor.

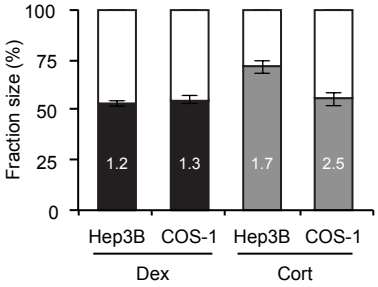

Figure 5.5: A similar pattern of YFP-GR's nuclear mobility in stably transfected Hep3B cells
SMM analysis of YFP-GR's nuclear mobility after treatment (3–6 h with 1 μM) with either dexamethasone or corticosterone was performed in Hep3B cells stably transfected with YFP-GR. These experiments were performed to check for effects of differences in cellular context and a lower level of YFP-GR expression on the mobility patterns. Both the size of the diffusing fraction (filled bars) and the diffusion coefficients (written in their corresponding bars in $\mu m/s^2$) were highly similar between COS-1 and Hep3B cells. COS-1 data is the same as in Figure 5.3. All groups: $n = 20$. Data is represented as total fit ± SEM (of 3 separate PICS analyses).

As expected, deletion of the DBD did affect the receptor's mobility (Figure 5.4). For corticosterone-bound GR, deletion of the DBD slightly increased the size of the diffusing fraction and completely prevents the longer binding events, resulting in two bound fractions with almost equal immobilization times: 0.5 ± 0.1 s (18 ± 3.9 %) and 0.6 ± 0.3 s (3 ± 1.5 %, Figure 5.4D). For dexamethasone-bound ΔDBD not all stable DNA-binding is lost; here 25 ± 2.7 % remains bound for 0.5 ± 0.1 s and even 9 ± 2.3 % remains bound for 1.4 ± 0.3 s. Dexamethasone-bound YFP-GR ΔDBD does show a large increase of the size of the diffusing fraction (from 44–55 % (wild type) to 76–66 % (ΔDBD)), and a ∼2-fold higher diffusion coefficient (Figure 5.4). Thus, deletion of the DBD induces less frequent and shorter DNA-binding for both dexamethasone and corticosterone bound GR, but a fraction of longer bound YFP-GR ΔDBD remains when bound to dexamethasone. Deletion of the DBD abolishes all direct binding of the GR to the DNA but leaves some of its indirect binding to DNA intact, which has been shown to occur through (direct or indirect) interactions with other transcription factors (Reichardt et al., 1998; Kassel and Herrlich, 2007). Therefore, the DNA-bound fraction of ΔDBD probably reflects indirect DNA-binding.

Deletion of the LBD prevents the ligand-induced conformational change that is required for any type of stable interaction with DNA. As expected, YFP-GR ΔLBD was the most mobile receptor variant, it had the smallest DNA-bound fraction (13.5 % to 18 % in SMM and FRAP respectively) with a single (short) binding state of 0.4 ± 0.1 s and a high diffusion coefficient (2.71 ± 0.08 $\mu m^2/s$; Figure 5.4). Most importantly, this DNA-binding deficient mutant indeed did not show any stably-bound fraction.

YFP-GR mobility is stable across cell lines and expression levels

In order to test whether overexpression or transient transfection had produced artifacts in our experiments, we stably transfected Hep3B cells with the same YFP-GR expression vector. The resulting cell line showed a much lower expression level of YFP-GR than that observed in the transiently transfected COS-1 cells. The DNA-binding dynamics were studied of corticosterone- and dexamethasone-bound YFP-GR in this cell line with SMM. Dexamethasone induced a diffusing fraction

			SMM		FRAP	
			Fraction size (%)	D (μm^2/s)	Fraction size (%)	Imm. time (s)
GR wt	Δ-Flu	Diffusing	46.3 ± 2.6	1.38 ± 0.11	43.0 ± 2.6	-
		Short	53.7 ± 2.6	0.050 ± 0.004	33.0 ± 2.1	0.8 ± 0.1
		Long			24.0 ± 2.2	2.9 ± 0.5
	Dexamethasone	Diffusing	55.1 ± 2.0	1.31 ± 0.13	44.0 ± 2.2	-
		Short	44.9 ± 2.0	0.030 ± 0.009	33.0 ± 2.6	0.7 ± 0.1
		Long			23.0 ± 2.6	2.3 ± 0.3
	Prednisolone	Diffusing	60.7 ± 3.1	2.20 ± 0.11	42.0 ± 2.5	-
		Short	39.3 ± 3.1	0.090 ± 0.008	36.0 ± 1.6	0.7 ± 0.1
		Long			22.0 ± 2.5	4.0 ± 0.8
	Cortisol	Diffusing	55.6 ± 3.5	1.77 ± 0.10	58.0 ± 2.0	-
		Short	44.4 ± 3.5	0.040 ± 0.003	19.0 ± 3.8	0.5 ± 0.1
		Long			23.0 ± 2.6	2.0 ± 0.0
	Corticosterone	Diffusing	74.1 ± 3.3	2.49 ± 0.24	66.0 ± 2.2	-
		Short	25.9 ± 3.3	0.080 ± 0.024	26.0 ± 3.7	0.6 ± 0.1
		Long			8.0 ± 2.5	1.2 ± 0.3
	RU486	Diffusing	69.1 ± 2.4	2.86 ± 0.11	66.0 ± 1.6	-
		Short	30.9 ± 2.4	0.140 ± 0.018	24.0 ± 3.1	0.5 ± 0.1
		Long			10.0 ± 2.6	1.4 ± 0.3
GR ΔAF-1	Dexamethasone	Diffusing	46.5 ± 1.9	0.61 ± 0.08	57.0 ± 3.0	-
		Short	53.5 ± 1.9	0.000 ± 0.006	18.0 ± 3.6	0.6 ± 0.1
		Long			25.0 ± 3.4	2.1 ± 0.4
	Corticosterone	Diffusing	64.7 ± 2.8	2.69 ± 0.08	62.0 ± 2.5	-
		Short	35.3 ± 2.8	0.050 ± 0.012	27.0 ± 4.0	0.6 ± 0.1
		Long			11.0 ± 2.3	1.6 ± 0.3
GR ΔDBD	Dexamethasone	Diffusing	75.6 ± 3.4	2.27 ± 0.15	66.0 ± 1.6	-
		Short	24.4 ± 3.4	0.010 ± 0.006	25.0 ± 2.7	0.5 ± 0.1
		Long			9.0 ± 2.3	1.4 ± 0.3
	Corticosterone	Diffusing	81.3 ± 1.0	2.37 ± 0.19	79.0 ± 3.1	-
		Short	18.7 ± 1.0	0.060 ± 0.004	18.0 ± 3.9	0.5 ± 0.1
		Long			3.0 ± 1.5	0.6 ± 0.3
GR ΔLBD	Dexamethasone	Diffusing	86.5 ± 1.9	2.71 ± 0.08	82.0 ± 3.3	-
		Short	13.5 ± 1.9	0.030 ± 0.010	16.0 ± 3.1	0.4 ± 0.1
		Long			2.0 ± 1.3	0.4 ± 0.3

Table 5.1: SMM and FRAP analyses of all YFP-GR and deletion mutants
Short, 'short' bound fraction; long, 'long' bound fraction; imm. time, average immobilization time; Δ-Flu, Δ-Fludrocortisone; Results are represented as best fit ± SEM (of three separate fits) for SMM and as average ± SEM of top 10 % fits for FRAP.

of 52.9 ± 1.6 % and a diffusion coefficient of 1.16 ± 0.08 μm^2/s in Hep3B cells (Figure 5.5). As expected, corticosterone treatment induced a more mobile YFP-GR, with a diffusing fraction of 71.6 ± 3.4 % and a D_{fast} of 1.70 ± 0.16 μm^2/s (Figure 5.5). These results were very similar to those obtained in COS-1 cells, indicating that our

results are not cell-type specific or affected by expression levels obtained by transient transfection.

5.4 Discussion

Here we report on a combination of SMM and quantitative FRAP analysis to characterize the intranuclear dynamics of the GR. In our SMM experiments, we find that single molecules of nuclear YFP-GR can be detected with high spatial and temporal resolution and that by subsequent data analysis two fractions of GR molecules are detected; a diffusing and a (DNA-)bound fraction. For all 11 treatment groups studied, this two-population model consistently fitted the experimental data with high accuracy. For dexamethasone-bound GR, $55\,\%$ of nuclear GR molecules are diffusing with a diffusion coefficient of $1.31 \pm 0.13\,\mu m^2/s$. The remaining $45\,\%$ show a > 40-fold lower diffusion coefficient, which fits the low, restricted mobility of DNA-bound molecules (Blainey et al., 2006; Elf et al., 2007; Li and Xie, 2011). To enable cross-validation with an established technique, we combined our SMM analysis with a second technique, FRAP. We analyzed the FRAP curves using established Monte Carlo simulations (Farla et al., 2004; van Royen et al., 2009b). To best describe the FRAP recovery curves we required two bound fractions (for most receptors), which differed 2–4 fold in their binding duration. The binding times of both bound fractions are orders of magnitude longer than the time scale used in our SMM experiments and these fractions combined represent the single bound fraction detected in SMM, providing two independent estimates of the size of this (combined) fraction. Within our 11 experimental conditions, the sizes of the combined bound fractions determined by SMM and FRAP showed an average difference of only $6.9 \pm 1.6\,\%$. This high level of consistency between the two independent techniques shows that a combination of techniques generates a reliable quantitative description of protein dynamics.

Combinations of FRAP and FCS have been reported earlier (Stasevich et al., 2010b; Mazza et al., 2012). Here, FSC and FRAP generally gave comparable estimates, although large discrepancies were found for binding times, due to laser irregularities. Recently, Mazza and colleagues reported on a similar combinational approach with FRAP and single-molecule microscopy, in their case also combined with FCS (Mazza et al., 2012). In this study the mobility of p53, a well-known transcription factor was assessed and single-molecule tracking was used to guide the choices in models used for FRAP and FCS quantitation. Wild type p53 showed a much smaller DNA-bound fraction ($\sim 20\,\%$) than agonist-activated GR does in our study, but in both studies mutations in the DNA-binding domains give a large reduction in size and residence time of the DNA-bound fractions (Mazza et al., 2012). In a recent study, Gebhardt et al. applied SMM on the GR as well, using reflected light sheet microscopy (Gebhardt et al., 2013). In this study unbound and dexamethasone-bound

GR and the ΔDBD mutant were analyzed. Their data are well in line with ours, especially the obtained values for the sizes of the diffusing and bound fractions and of binding times (Gebhardt et al., 2013). Discrepancies exist in the analysis of the diffusing fraction. Gebhardt et al. found two diffusing fractions, whereas we only detect one. As shown by Mazza et al., it is likely that any diffusion coefficient is a simple representation of the more complex nature of the continual scale of true transcription factor diffusion (Mazza et al., 2012).

Ligand structure affects the DNA-binding profile of nuclear GR

We observed profound differences in the nuclear dynamics of the GR depending on the ligand it was bound to (Figure 5.3), even among agonists. For example, the synthetic GR agonists dexamethasone and Δ-fludrocortisone induce a larger DNA-bound fraction with longer residence times than the naturally occurring agonists cortisol and corticosterone. Structure-function studies showed that the 17-hydroxyl, and 9-fluoro groups and the 1,4-pregnadien structure of the A ring of these steroids were involved in the increased DNA binding of GR. We further showed that the effect of the 9-fluoro group depends on the presence of phenylalanine at position 623 of the GR LBD, the amino acid it is known to interact with (Bledsoe et al., 2002). This phenylalanine residue, like the glutamine residue at position 642, which interacts with 17-hydroxyl group, is located in a region of the LBD that has been shown to be involved in receptor dimerization (Bledsoe et al., 2002). It may therefore be suggested that these specific interactions shape the receptor into a conformation that favors receptor dimerization, and that these dimers have higher DNA binding affinity. We have previously suggested a similar model for AR dimerization and DNA binding (van Royen et al., 2012).

Many of these structural elements also affect the affinity of the ligand and it could therefore be argued that the affinity of the ligand determines the receptor mobility. However, affinity and mobility are not always correlated. In a previous study we have shown that the 16-hydroxy group of triamcinolone dramatically decreases the binding affinity for GR, but leaves GR mobility unaffected (Schaaf and Cidlowski, 2003; Schaaf et al., 2005). Furthermore, mechanistically it is unlikely that ligand affinity is a determinant of receptor mobility since all ligands are administered at above saturating concentrations (Schaaf and Cidlowski, 2003). Finally, ligand dissociation rates are in the order of minutes (corticosterone) to hours (dexamethasone) (Munck and Foley, 1976; Meijsing et al., 2007), whereas the immobilizations of the receptor observed in this study are in the order of seconds.

A model of GR-DNA interactions

Interestingly, our data shows a strong correlation between different components of the mobility pattern. Immobilization times correlate to the size of the bound fractions, but more surprisingly, we also found that a low frequency and duration of

binding events correlated with a higher diffusion coefficient throughout our different experiments. Thus, where antagonist-bound or low-affinity agonist bound GR, and the ΔDBD and ΔLBD mutants were all associated with a low frequency of DNA-binding, these same receptors all showed a high diffusion coefficient (1.5 to 2-fold higher than that of highest-potency agonist bound GR, see Table 5.1). This suggests that all components of the mobility pattern are associated with each other and presumably are representations of a same biological phenomenon, i.e. DNA-binding. A plausible explanation could be that changes in the diffusion coefficient are due to DNA-binding events shorter than the temporal resolution of our SMM experiments ($\sim$6 ms), which result in a decreased effective diffusion coefficient as long as the system is in equilibrium. Alternatively, reduced diffusion coefficients can be caused by an increased size of the diffusing protein complex (e.g. through increased co-factor binding affinity).

Thus, for agonist-bound GR we identified three possible DNA-binding events: frequently in a very transient manner (< 6 ms), intermitted with transient binding ($\sim$0.5 s) and occasionally more stable interactions (> 1 s). This fits well with the idea that steroid receptors and other transcription factors search the DNA by different forms of low affinity DNA interactions and are only occasionally bound for longer time periods at their high-affinity target sites. Indeed, steroid receptors do not show competition for high-affinity binding sites, and in fact seem to do the opposite (assisted loading), suggesting that high-affinity DNA-binding cannot make up a large population (Voss et al., 2011). Multiple *in vitro* studies and theoretical modeling approaches have suggested that frequent low-affinity interactions with DNA increase the efficiency of transcription factor target finding, because it keeps the transcription factor in close proximity of open DNA (Gowers et al., 2005; Elf et al., 2007; van den Broek et al., 2008). We suggest that the more transient interactions identified in our quantitative analysis represent non-specific DNA binding and that the longest DNA-binding events represent specific DNA binding.